Metallomics

Accepted Manuscript

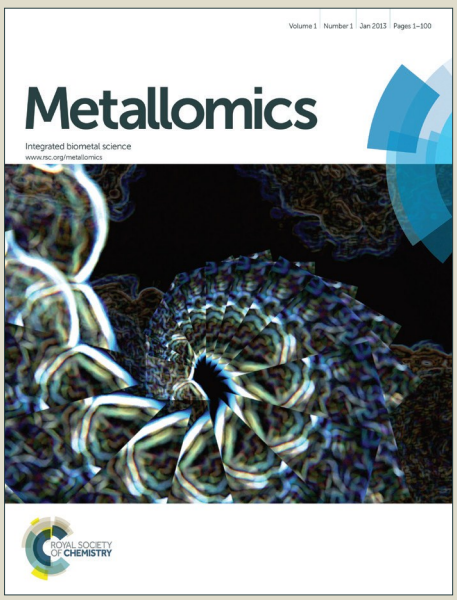

ROYAL SOCIETY OF CHEMISTRY

www.rsc.org/metallomics

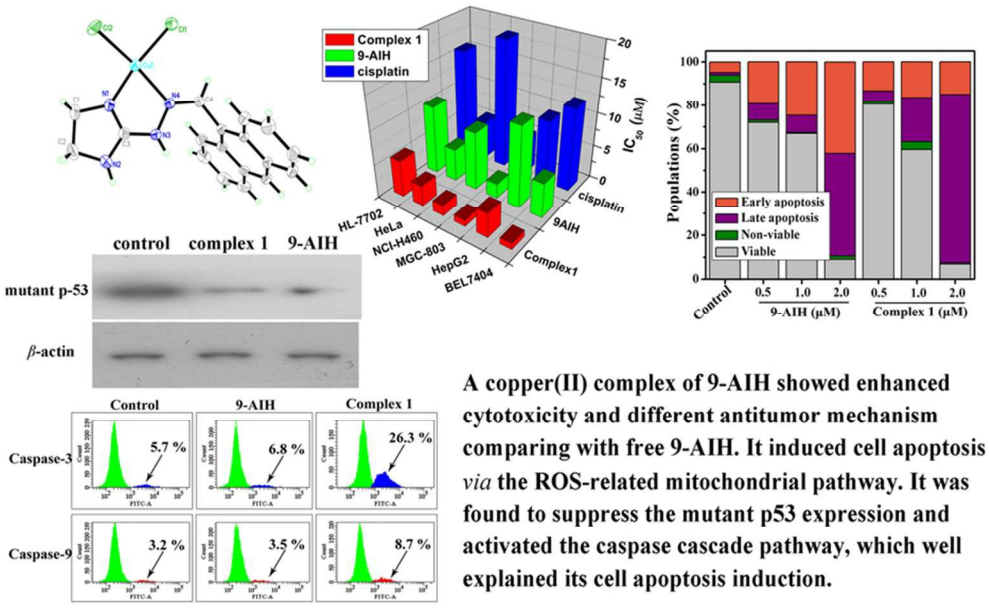

A copper(II) complex of 9-AIH showed enhanced cytotoxicity and different antitumor mechanism comparing with free 9-AIH. It induced cell apoptosis *via* the ROS-related mitochondrial pathway. It was found to suppress the mutant p53 expression and activated the caspase cascade pathway, which well explained its cell apoptosis induction.

80x51mm (300 x 300 DPI)

Cite this: DOI: 10.1039/c0xx00000x

www.rsc.org/xxxxxx

ARTICLE TYPE

Synthesis and antitumor mechanism of a copper(II) complex of anthracene-9-imidazoline hydrazone (9-AIH)

Qi-Pin Qin, Yan-Cheng Liu*, Hai-Lu Wang, Jiao-Lan Qin, Feng-Jie Cheng, Shang-Feng Tang, and Hong Liang*

Received (in XXX, XXX) Xth XXXXXXXXX 20XX, Accepted Xth XXXXXXXXX 20XX
DOI: 10.1039/b000000x

A new anthracycline derivative, anthracene-9-imidazoline hydrazone (9-AIH) was synthesized and selected as an antitumor ligand to afford a copper(II) complex of 9-AIH, *cis*-[$Cu^{II}Cl_2$(9-AIH)] (**1**). Complex **1** was structurally characterized by IR, elemental analysis, ESI-MS and single crystal X-ray diffraction analysis. By MTT assay, **1** showed overall higher *in vitro* cytotoxicity than 9-AIH towards a panel of human tumour cell lines, with IC_{50} values from 0.94 ~ 3.68 μM, in which the BEL-7404 cell line was the most sensitive one to **1**. By spectral analyses and gel electrophoresis, the DNA binding affinity of 9-AIH and **1** was discussed. 9-AIH was suggested to bind with DNA in an intercalative mode, with a quenching constant of 1.04×10^4 M^{-1} on the EB-DNA complex. While for **1**, both intercalative and covalent binding modes were suggested. By flow cytometry, **1** was found to block the cell cycle of BEL-7404 cells in a dose-dependent mode, in which it induced the G_2/M phase arrest at 0.5 μM and induced the S phase arrest at higher concentrations of 1.0 or 2.0 μM. From the cellular morphological observations under different fluorescence probe staining, a dose-dependent manner of **1** to induce cell apoptosis in the late stage was suggested. Comparatively, equivalent apoptotic cells respectively in the early and late stage were found when incubated with 2.0 μM of 9-AIH. The mitochondrial membrane potential measured by JC-1 staining and the ROS generation in cells detected by DCFH-DA probe suggested that the cell apoptosis induced by **1** might undergo the ROS-related mitochondrial pathway. Accordingly, the mutant p53 expression was found to be suppressed and the caspase cascade (caspase-9 / 3) was consequently activated by **1**. This action mechanism for **1** in the BEL-7404 cells was unique and was not found in the presence of 9-AIH under the same condition, indicating their different antitumor mechanism. Furthermore, the *in vivo* acute toxicity of **1** tested on mice indicated that **1** should be a high cytotoxic antitumor agent, with the LD_{50} value in the range of 32~45 mg/kg, which is much higher than 9-AIH. From the results above, the central Cu(II) of **1** in the coordinated mode with 9-AIH was believed to play a key role to exert both the high cytotoxicity and the effective antitumor mechanism.

1. Introduction

In the clinical chemotherapy for a broad spectrum of carcinomas, the anthracyclines rank among the most effective anticancer drugs ever developed since the 1970s. Daunorubicin and doxorubicin were the first naturally derived anthracyclines, followed by the derivatives such as epirubicin, idarubicin, mitoxantrone, et al [1]. The advantages of anthracyclines include the high cytotoxicities, effective tumour growth inhibitions and the more broad-spectrum antitumor activities, such as against the leukemia, lymphoma, breast carcinoma, cervical carcinoma, hepatoma, et al, than most of the other antitumor drugs [2]. It is generally accepted that the significant antitumor activities of the anthracyclines can be attributed to their significant inhibitions on the topoisomerase II activity and DNA damage [3]. However, the clinical uses of the anthracyclines are also heavily limited due to their severe cardiac toxicity, which is believed to be closely related to the characteristic anthraquinone structure of the anthracyclines [4]. The reduction of the quinonoid carbonyl (C=O) will give the reactive oxygen species (ROS), which will damage the cardiac cells [5]. Bisantrene, as a new developed anthracyclines derivative *via* organic synthesis, was launched into the American market in 1991 for the cancer treatment. As a satisfactory attempt to avoid the cardiac toxicity of anthracyclines, the anthraquinone moiety, as well as the amino sugar moiety, was not found in the structure of bisantrene, as shown in Scheme 1. Bisantrene can be synthesized by the reaction of 9,10-anthraldehyde and two fold of 2-hydrazino-2-imidazoline bromide, which affords a new anthracene hydrazone structure. It has been accepted that bisantrene exerts its significant antitumor efficacy by inhibiting the topoisomerase II activity *via* intercalative binding with DNA [6]. Although it has been dropped out from the first-line chemotherapy in the recent years due to its severe hematic and hepatic toxicities, the designed anthracene hydrazone structure of bisantrene for developing new type of

anthracycline drugs is still inspiring and significative.

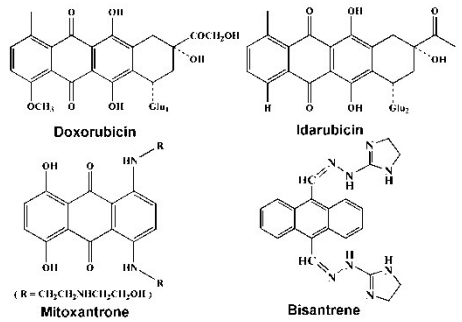

Scheme 1. The chemical structures of some typical anticancer anthracyclines.

On the other hand, inspired by the success of cisplatin as an effective inorganic anticancer agent, researches for developing metal-based anticancer complexes bearing functional ligands are still in the ascendant. Copper as a human essential element has attracted many inorganic chemists to address copper(II) complexes with the aim for medical applications, due to its significant bioactivity and redox reactivity [7,8]. For example, Lovejoy et al. studied the lysosomal-related antitumor activity of a kind of thiosemicarbazone mediated by formation of a redox-active copper complex [9]. Boutaleb-Charki et al. reported a series of copper(II) complexes bearing triazolo pyrimidine ligands, which showed enhanced anti-parasitic activities by balancing the level of NAD^+/NADH in the energy metabolism of the parasites [10]. Sun et al. discussed the oxidative DNA cleavage mediated by a series of copper(II) complexes [8].

The imine derivatives, such as Schiff base, is a class of *N*-containing ligands with significant bioactivities [11,12]. The copper(II) complexes bearing this kind of ligand have been extensively studied for their enhanced pharmacological activities, which can be correlated to the strong DNA intercalation or oxidative DNA cleavage [13], as well as the activation on the mitochondrial pathway for cell apoptosis *via* the redox activity of the copper(II) centre [14,15]. The anthracene hydrazone can be also considered as a kind of imine derivative with potential antitumor activity. However, few metal complexes bearing anthracene hydrazone as ligand were reported till now [16]. And the further studies on the molecular level for the cell apoptosis induced by these complexes were much more insufficient and need to be explored in depth.

In the present study, an anthracycline derivative, anthracene-9-imidazoline hydrazone (9-AIH), which referenced and was inspired by the structural advantages of bisantrene, was synthesized as a potential antitumor compound. And a new copper(II) complex, *cis*-[$Cu^{II}Cl_2$(9-AIH)] (**1**), was firstly synthesized and structurally characterized. Based on the prominent *in vitro* cytotoxicity of **1** against the BEL-7404 tumor cell line by MTT assay, its antitumor mechanism concerning the cell cycle arrest and cell apoptosis pathway was explored and discussed by means of confocal laser scanning microscope, flow cytometry and western blotting assay. The acute toxicity of **1** *in vivo* was further evaluated for better explanation. While the 9-AIH ligand was also studied for the first time for comparison.

2. Results and discussion

2.1. Synthesis and structural characterization of 1

2.1.1. Structural characterization in crystalized state

The synthetic route of 9-AIH and **1** was shown in Scheme 2, with 9-anthraldehyde and 2-hydrazino-2-imidazoline hydrobromide as starting materials. They were both fully structurally characterized. The crystal structure of **1** was also resolved by the single crystal X-ray diffraction analysis, which demonstrated that it belonged to the monoclinic crystal system with space group $P2_1/c$. The ORTEP view of **1** with labeled atoms was shown in Figure 1. For **1**, the copper(II) was four-coordinated by two Cl atoms and one 9-AIH anthracene hydrazone ligand *via* the 3-N of imidazole and the imine N atom, to form an electroneutral transition metal complex. The N1 and N4 atoms of the 9-AIH ligand bidentated the Cu(II) centre and the two Cl atoms coordinated to Cu(II) in a cis-mode, by which the planar quadrilateral coordination geometry was formed. The Cu1–N1 and Cu1–N4 bond lengths were 1.931(3) Å and 2.101(3) Å, respectively, which were within the normal range of the coordinative bonding between Cu(II) and N atom. The bond lengths of Cu1–Cl1 (2.2661(11) Å) and Cu1–Cl2 (2.2781(9) Å) were much higher than those of the Cu–N bonds in **1**, indicating the coordinated Cl atoms more easily dissociated from the Cu(II) centre by hydrolysis. In the crystal structure of **1**, ethanol molecules as solvent were co-crystalized in the molar ratio of [**1**]:[ethanol] = 1:1, which has been considered for calculation in the following biological experiments. (It should be noted that the ethanol in the crystal structure is disordered.) molecule and the Cu(II) also existed (Cu1–O1, 2.585 Å). In this solid state of **1**, a three-dimensional supramolecular structure was The weak interaction between the O atom of each ethanol formed by the N—H ··Cl and C—H ··Cl hydrogen bonding and π–π stacking between the neighboring anthracene groups (see Figure S1). The details of the crystallographic data and structural refinement parameters were summarized in Table 1. Selected bond lengths and bond angles were listed in Table S1.

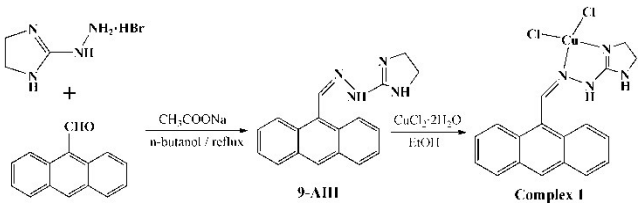

Scheme 2. The synthetic route of 9-AIH and complex **1**.

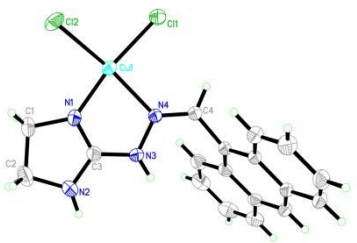

Figure 1. An ORTEP view of complex **1**, [$Cu^{II}Cl_2$(9-AIH)]•C_2H_5OH. The selected atoms were labeled and drawn as thermal ellipsoids at the 30% probability, and the disordered ethanol as solvent molecule in the crystal unit was omitted for clarity.

Table 1. Crystal data and structure refinement parameters for complex **1**, $[Cu^{II}Cl_2(9\text{-AIH})]\bullet C_2H_5OH$, in which the C_2H_5OH is disordered.

Chemical formula	$C_{20}H_{22}Cl_2CuN_4O$
Formula Weight	464.82
Crystal system, space group	Monoclinic，$P2_1/c$
Unit Cell Dimensions	a/ Å = 11.3306(3), α/ °= 90.00
	b/ Å = 14.0417(3), β/ °= 106.842(4)
	c/ Å = 13.3887(5), γ/ °= 90.00
Volume (Å^3)	2038.78(11)
Crystal size (mm^3)	0.40 ×0.20 ×0.12
Temp (K)	293(2)
Z	4
D_{calc} (g.cm^{-3})	1.514
θ range for data collection	5.8 to 52.74 °
$\mu_{absorp.}$ (mm^{-1})	1.351
Limiting indices	$-14 \le h \le 14, -14 \le k \le 17, -16 \le l \le 16$
F (000)	948
Reflections collected / unique	16428
Independent reflections	4167 [R(int) = 0.0301]
Data/restraint/parameters	4167 / 0 / 257
R (all data)	R_1 = 0.0599, ωR_2 = 0.1347
R [I>2σ (I)]	R_1 = 0.0479, ωR_2 = 0.1254
Goodness-of-fit on F^2	1.047
Largest diff. peak/hole(e/Å^3)	0.801 / –0.500

2.1.2. Solution chemistry study

Analyzing the existing species of **1** in the solution state will help to confirm the effectual species for its antitumor activity, for which the UV-vis, HPLC and ESI-MS analyses were performed. The solution chemistry of **1** in aqueous solution was primarily analyzed by means of UV-Vis spectroscopy and HPLC, as shown in Figures S2 and S3, respectively. The UV-Vis spectrum of **1** in tris buffer solution (pH = 7.35, containing 1% DMSO) for 24 h was shown in Figure S2. It can be found that the UV-Vis spectral character of complex **1** retained without new emerged absorption peaks, suggesting the stability of the coordinating state of **1** over 24 h. The stability of **1** was also monitored by HPLC using a mobile phase of methanol/H_2O (85/15) for 24 h, as shown in Figure S3, which also suggested the stability of **1** in its coordinated state over 24 h in an aqueous solution. Both the results indicated that the coordinating state of 9-AIH to Cu(II) could retain under the physiological conditions, which was in agreement with the result of ESI-MS analysis as the following. As shown in Figure S4, the ESI-MS analysis of **1** incubated in tris buffer solution (containing 5% DMSO) for 0 h showed a maximum abundance of m/z = 464.05 for $[Cu^{II}Cl(9\text{-AIH}) + DMSO]^+$. It suggested that one of the chloridion of **1** tended to be replaced by a DMSO solvent molecule in DMSO stock solution. The maximum abundance of **1** for 24 h was found to be m/z = 386.4 $[Cu^{II}Cl(9\text{-AIH})]^+$, in which the DMSO molecule dissociated into the aqueous solution. It confirmed the predominant coordinated species of **1** under the physiological condition at 24 h, which ensured the adequate cell uptake of **1** during the time course for MTT assay.

Therefore **1** in the required time could retain a planar coordinated geometry with a positive charge under the physiological conditions. This positive charged planar structure of **1** can expect its more significant antitumor activity than 9-AIH, due to its proposed higher DNA binding affinity.

2.2 In vitro cytotoxicity

The *in vitro* cytotoxicities of 9-AIH and **1** were primarily evaluated by MTT assay towards a panel of human tumor cell lines including BEL-7404, HepG2, MGC80-3, NCI-H460, HeLa, and the normal liver cell line HL-7702. As listed in Table S2, the preliminary screening at 20 μM showed that **1** was more cytotoxic than 9-AIH and cisplatin against all the cell lines, while $CuCl_2$ alone did not show considerable activity. The further IC_{50} values of **1**, 9-AIH and cisplatin were listed in Table 2. **1** showed much lower IC_{50} values (0.94~3.68 μM) against the five tumour cell lines than 9-AIH (2.23~12.13 μM) and cisplatin (5.43~18.89 μM). BEL-7404 was the most sensitive tumor cell line to **1** with IC_{50} value of 0.94 μM, which were approximate 6 and 13 folds increments comparing with the free 9-AIH and cisplatin, respectively. It strongly suggested the positive synergistic effect of **1** by coordinating 9-AIH as a functional group to copper(II). And the significant cytotoxicity of **1** was also satisfying comparing with other reports on the copper(II) complexes bearing similar ligands [9,17].

It should be noted that the cytotoxicity of **1** against the normal liver cell HL-7702 was also higher than those of 9-AIH and cisplatin by 2~3 folds, which is consistent with the high cytotoxicity of **1**. However, the cytotoxicity of **1** against BEL-7404 was almost 6 times as against the HL-7702 normal cell line, suggesting the satisfying high selectivity of **1** towards the BEL-7404 tumor cell line [18].

Table 2. IC_{50}[a] (μM) values of 9-AIH and complex **1** against the five typical human tumor cell lines as well as the human normal liver cell line HL-7702.

Compounds	9-AIH	Complex **1**	Cisplatin [b]
BEL-7404	5.23±0.77	0.94±0.23	12.41±0.38
HepG2	12.13±0.61	3.68±0.12	9.48±0.35
MGC80-3	2.23±0.12	0.96±0.25	5.43±0.45
NCI-H460	8.69±0.12	1.65±0.18	18.89±1.02
HeLa	4.86±0.43	3.14±0.16	5.79±1.02
HL-7702	10.24±0.42	5.51±0.12	15.67±0.32

[a] IC_{50} values are presented as the mean ± SD (standard error of the mean) from five independent experiments. [b] Cisplatin was dissolved at a concentration of 1 mM in 0.154 M NaCl [18].

2.3 DNA binding studies

DNA is generally regarded as the primary target for many antitumor agents [19,20]. The antitumor metal complexes targeting DNA have been extensively reported, especially those bearing aromatic planar ligands [21]. DNA has been proven to be the primary intracellular target for the anthracyclines as well as its derivatives, such as bisantrene [22,23]. Therefore, the DNA binding properties of 9-AIH and **1** should be confirmed to provide direct evidence to explain their antitumor mechanisms. For this purpose, their DNA binding properties were primarily discussed by means of UV-vis and fluorescence spectral analysis as well as agarose gel electrophoresis assay.

2.3.1 Electrostatic interaction by UV-vis spectral analysis

Sodium dodecyl sulphate (SDS) is suggested as a probe instead of DNA to investigate the potential electrostatic interactions between small molecules and DNA, due to the polymeric SDS

acting as an appropriate substitute for DNA polyanionic backbone. By UV-vis spectral analysis, the effect of SDS added into the aqueous solution of **1** or 9-AIH was shown in Figure 2, respectively. The significant hypochromic effects, along with the observed isosbestic point at *ca.* 260 nm, were found in the UV-vis spectra of both **1** and 9-AIH upon the addition of SDS, which implied the electrostatic interactions existed between DNA and **1** (or 9-AIH) [24]. It can be explained from the above ESI-MS analysis of the **1**, which suggested the tendency to generate the cationic species, $[CuCl(9\text{-}AIH)]^+$, in aqueous solution. As to 9-AIH, its protonated species, $[9\text{-}AIH + H]^+$, is more easily formed in aqueous solution.

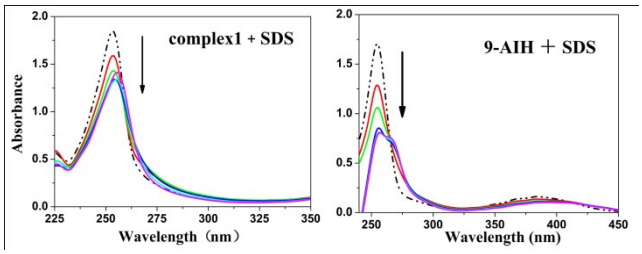

Figure 2. UV-vis absorption spectra of complex **1** and 9-AIH at 20 μM in the absence (dashed line) and presence (solid lines) of increasing amounts of SDS in 1% DMSO containing TBS buffer solution.

2.3.2 Fluorescence emission titration

The fluorescence spectral analysis was also performed for DNA binding studies in a competitive binding mode with EB, which is a classic intercalative probe to DNA emitting characteristic fluorescence at 590 nm [25]. In this experiment, the [EB]/[DNA] was set to be 1:10 to ensure sufficient DNA binding sites for EB. As shown in Figure 3, EB-DNA complex gave the characteristic fluorescence emission at *ca.* 590 nm when excited at 350 nm, indicating the EB molecules intercalated between the adjacent base pairs of DNA. The addition of increasing amounts of 9-AIH led to moderate and regular fluorescence quenching of EB, with a total quenching ratio of 51.9% when the [9-AIH]/[EB]/[DNA] ratio reached 10: 1: 10. It suggested the competitive binding between 9-AIH and EB with DNA, which was regarded as a direct evidence for the intercalative binding property of 9-AIH. Using the classic Stern-Volmer quenching equation, the quenching constant, K_q, for 9-AIH was calculated to be 1.04×10^4, indicating its relatively weak DNA intercalative binding ability comparing with EB [26].

While the addition of **1** under the same condition showed higher efficiency to quench the fluorescence of EB, with a total quenching ratio of 77.8% when the [**1**]/[EB]/[DNA] ratio reached 10:1:10. It suggested the higher DNA binding affinity of **1** than 9-AIH when competing with EB. However, it should be noted that the inset plot of I_0/I vs. [DNA] for **1** did not fit the Stern-Volmer linear equation, and the up-tilting towards the Y-axis was observed, which was regarded as the dual quenching mechanism [27]. Therefore **1** might interact directly with EB to quench its fluorescence emission, suggesting that the central Cu(II) of **1** acted as a key role to facilitate the DNA binding [28,29].

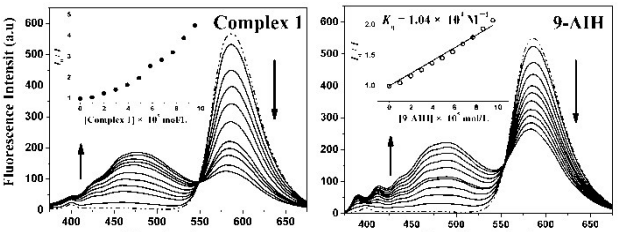

Figure 3. Fluorescence emission spectra of EB bound with ct-DNA ([DNA]/[EB] = 100 μM / 10 μM) under the addition of 1 and 9-AIH with increasing concentrations, respectively.

2.3.3 Agarose gel electrophoresis assay on plasmid DNA

The interaction mechanism of **1** and 9-AIH with DNA was further examined by agarose gel electrophoresis assay, as shown in Figure 4. After the pUC19 plasmid DNA was treated by **1** of increasing concentrations from 20 to 100 μM, the mobility of the supercoiled DNA (form I) decreased to some extent, suggesting the intercalative binding of **1** with DNA, as did the classic DNA intercalator, EB [30]. The presence of 100 μM of **1** turned most of the supercoiled DNA to the linear DNA (form III). It can be ascribed to the redox-active cleavage ability of cooper(II) centre of **1** on DNA, which were found in quite some reported copper(II) complexes showing antitumor activities [9,31]. While the presence of 9-AIH under the same condition only slightly decreased the mobility of the supercoiled DNA, and no conformal transformation was found, suggesting the simple intercalative binding mode of 9-AIH to DNA [32].

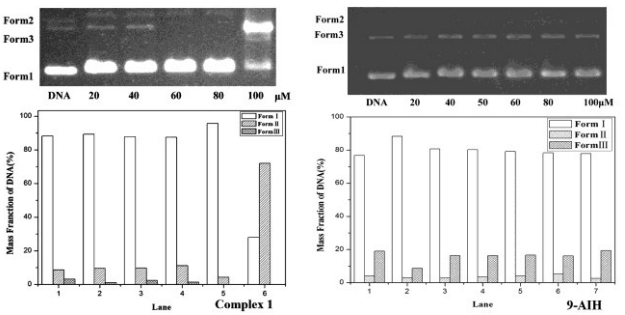

Figure 4. Agarose gel electrophoresis diagrams showing the mobility of various forms pUC19 DNA (0.5 μg/μL) when interacted with complex **1** (left) or 9-AIH (right) with increasing concentrations from 20 to 100 μM in TBE buffer (pH = 8.3) at 37 ℃. Quantification of the electrophoresis bands of DNA originating from Form I, II, III was summarized at the bottom by the OD values of each band, which were standardized to 100% for each individual lane.

In summary, the UV-vis spectral analysis using SDS as probe suggested **1** might interact with DNA by electrostatic attraction. This will facilitate the higher intercalative binding affinity of **1** than 9-AIH towards DNA, which was confirmed by the fluorescence spectral analysis and electrophoresis assay. Furthermore, the electrophoresis assay indicated that **1** also showed DNA cleavage ability, most probably due to the redox state of the copper(II) centre. These findings well agreed with the higher *in vitro* cytotoxicity of **1** than 9-AIH towards most of the tested tumor cell lines, in which the central copper(II) should play a key role.

2.4 Cell cycle assay

The high cytotoxicity *in vitro* and the significant DNA binding

affinity of the copper(II) complex **1** of 9-AIH were attractive enough to explore the antitumor mechanism in details on the cellular and molecular levels. Primarily, the DNA binding affinity of **1** led us to study its effect on blocking the cell cycle by flow cytometry, and the most sensitive tumor cell line BEL-7404 towards **1** was selected for investigation. As shown in Figure 5, after the BEL-7404 cells were incubated with increasing concentrations (0.5, 1.0, 2.0 μM) of **1** for 48 h, the population of the cells in G1 phase decreased from 50% to no more than 15%. In the presence of **1** at 0.5 μM, the population of the G_2/M phase cells dramatically increased to 70%; while at higher concentrations as 1.0 and 2.0 μM of **1**, the S phase cells increased to *ca.* 60%, and the G_2/M phase cells fell back to 21~26%. It can be affirmed that the characteristic S phase cell cycle arrest of the BEL-7404 cells when treated by **1** at 1.0 and 2.0 μM. However, the significant G_2/M phase cell cycle arrest treated by **1** at 0.5 μM still remained to be discussed. For comparison, the cell cycle assay of the BEL-7404 cells incubated with 9-AIH under the same condition was also studied. From the results in Figure 1, it showed different effect for 9-AIH to block the cell cycle of BEL-7404 cells. With the increasing concentrations of 9-AIH, the population of G_2/M phase cells increased steadily from 14% till to 79% (for **1** at 2.0 μM), which clearly indicated the G_2/M phase cell cycle arrest by 9-AIH in a dose-dependent manner. From these results, we assumed that the antitumor mechanisms of 9-AIH and **1** in the BEL-7404 tumor cells were different, which were also indicated by the followed cell apoptosis assay.

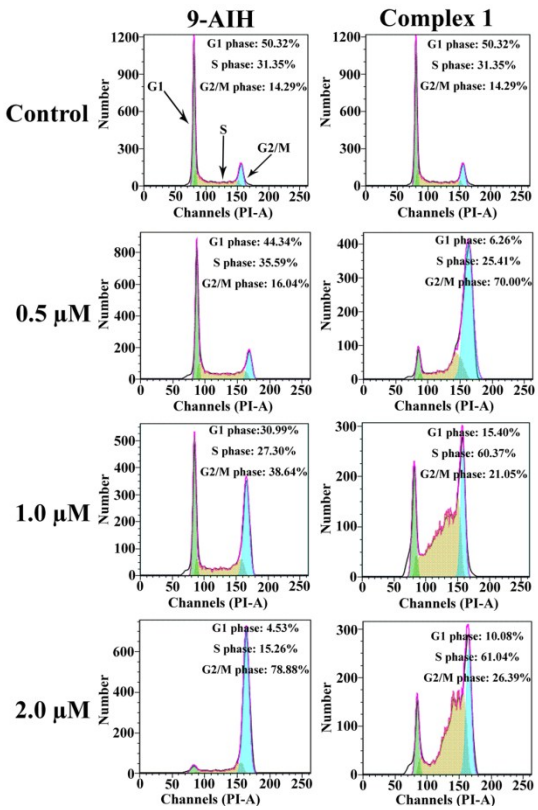

Figure 5. Cell cycle distribution of the BEL-7404 cells when treated by 9-AIH and complex **1** for 48 h with increasing concentrations (0.5, 1.0, 2.0 μM), respectively. Data on each sample represent the percentages of the cells in G1, S and G2/M phase.

2.5 Cell morphological observation for cell apoptosis induction

The cell cycle arrest is closely related with the cell apoptosis, and plays a non-trivial role in the cell apoptosis of tumor cells [33]. So the possible cell apoptosis in the BEL-7404 cells induced by 9-AIH or **1** was primarily studied by observing the changes in the cell morphology after the cells were stained by the membrane-permeable Hoechst33258 and AO/EB, respectively. As shown in Figure 6, under the visual field of 100× magnifications, it was found that the cell morphology of the BEL-7404 cells in the control group remained regular with round contours. However, the changes on the cell morphology can be clearly observed after the cells were incubated with 9-AIH or **1**. In the presence of **1** even at low concentration of 1.0 μM, quite some of the cells showed characteristic apoptosis, such as the contours of the cells became irregular, more nuclei appeared hyper-condensed (as bright blue fluorescence indicated) and some apoptotic bodies were found. Especially, the population of the apoptotic cells containing condensed nuclei and chromatin increased significantly in the presence of 2.0 μM of **1**, suggesting the dose-dependent manner of **1** to induce apoptosis. Under the same condition, the similar morphological changes on the BEL-7404 cells were also found when they were treated with 9-AIH. Furthermore, as shown in Figure 7, the AO/EB staining gave clearer differentiation on 9-AIH and **1** to induce the cell apoptosis at the same concentration of 1.0 μM, from which it can be found that **1** induced more cell apoptosis (as orange fluorescence indicated) than did 9-AIH.

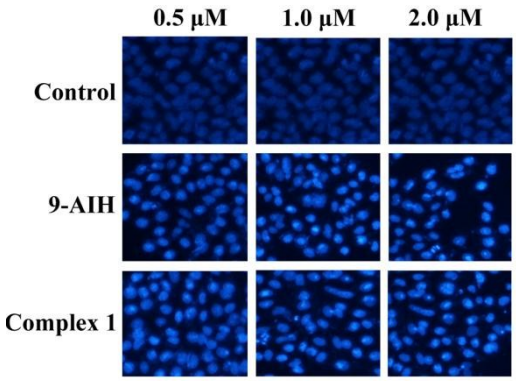

Figure 6. Morphological changes in the nuclei (typical of apoptosis) of BEL-7404 cells treated by 0.5, 1.0 and 2.0 μM of 9-AIH and complex **1** for 24 h, respectively, and stained by Hoechst 33258. Selected fields illustrating condensed chromatin (white arrow heading) as occurrence of cell apoptosis were shown. Images were acquired using a Nikon Te2000 deconvolution microscope (magnification 100×).

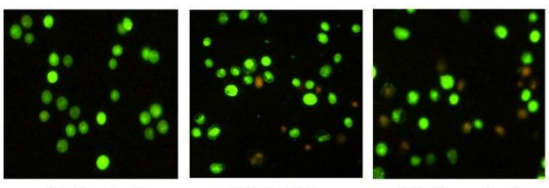

Figure 7. Apoptosis observation of BEL-7404 cells treated by 1.0 μM of 9-AIH and complex **1** for 24 h, respectively, and stained by AO/EB. Selected fields illustrated the corresponding live cells (green), apoptotic cells and death cells (orange or red). Images were acquired using a Nikon Te2000 deconvolution microscope (magnification 200×).

2.6 Cell apoptosis assay by flow cytometry

By examining the phosphatidylserine exposed outside on the cell membrane surface, which can be double stained by Annexin V and PI for visualization, the cell apoptosis induction by 9-AIH or **1** was detailed assessed by flow cytometry. As shown in Figure 8, the incubation of the BEL-7404 tumor cells with increasing concentrations of **1** led to the dramatic increase of apoptotic cells (Q2 zone). The maximum percentage for the apoptotic cells at the late stage was 78% in the presence of **1** at 2.0 μM, along with the 15% cells at the early stage of apoptosis. In contrast, the presence of 9-AIH at 2.0 μM induced obvious cell apoptosis both at the late stage (47%, Q2 zone) and the early stage (42%, Q3 zone).

Furthermore, the BEL-7404 cells incubated with 20 μM of each compound were also examined for cell apoptosis induction (see Figure S5), in order to determine whether the compound induced the cell apoptosis in a reliable dose-dependent mode. As indicated in Figure S5, both compounds could almost exhaustively induce cell apoptosis at the late stage, with the percentage of *ca.* 90% for 9-AIH and 95% for **1**. For the intuitive comparison on both compounds, the quantitative histogram for the cell apoptosis in BEL-7404 cells induced by gradient concentrations of **1** and 9-AIH was also presented in Figure 9. Viewed from the results, it suggested that **1** and 9-AIH did not show the same mode to induce cell apoptosis in BEL-7404 cells, which may be closely correlated with their different manners to induce the cell cycle arrest. And obviously, complex **1** showed much higher ability to induce apoptosis in BEL-7404 cells.

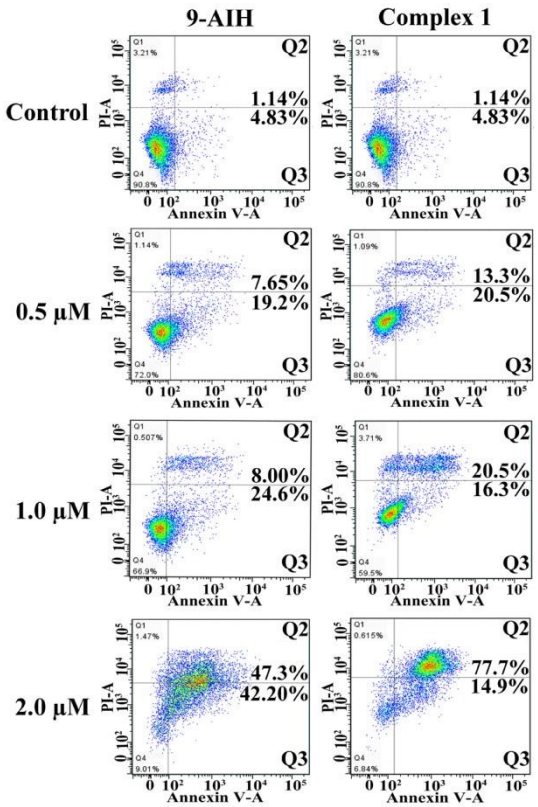

Figure 8. The cell apoptosis in BEL-7404 cells induced by 9-AIH and complex **1** at 0.5, 1.0, 2.0 μM for 24 h, respectively, which was examined by FACS analysis using the PI and FITC-Annexin V double staining.

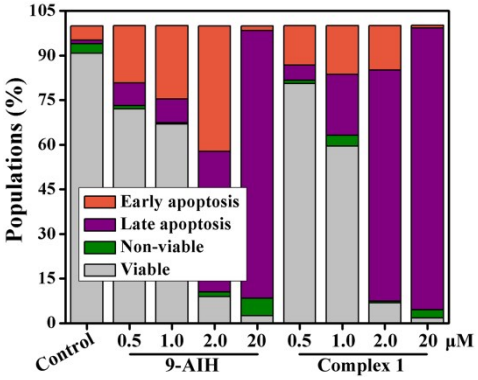

Figure 9. Populations for cell apoptosis of BEL-7404 cells treated with 9-AIH and complex **1** for 24 h comparing to the untreated cells.

2.7 The mitochondrial membrane potential assay for cell apoptosis

The loss of mitochondrial membrane potential ($\Delta\psi$) is generally accepted as a key factor in the early-stage apoptotic pathway, by which the mitochondrion is becoming a more important intracellular antitumor target and has been regarded to be high important in controlling the cell apoptosis [34]. To further confirm the cell apoptosis induction by **1** or 9-AIH, the changes on the mitochondrial membrane potential in the BEL-7404 cell were detected by using the fluorescent probe, JC-1. In the living cells, JC-1 probe molecules existing in the mitochondria matrix of cytosol tend to accumulate to form J-aggregates, which will emit orange fluorescence. While in the apoptotic or necrotic cells, owing to the loss of $\Delta\psi$, JC-1 molecules will exist in the monomeric form and stain the cytosol to emit green fluorescence. The changes on the $\Delta\psi$ in BEL-7404 cells indicated by JC-1 staining were shown in Figure 10. It was found that all the cells in the control group emitted orange fluorescence under the JC-1 staining, suggesting the coupled mitochondria with a normal $\Delta\psi$. However, the cells incubated with **1** of increasing concentrations from 0.5, 1.0 to 2.0 μM emitted more and more intensive green fluorescence, indicating the typical property of cell apoptosis induced by **1** in a dose-dependent manner. The results suggested that 9-AIH also induced significant cell apoptosis in a dose-dependent manner. But the effect of 9-AIH on inducing the cell apoptosis was still relatively weak than that of **1**, as compared in Figure 10 under the same concentration. Anyway, these results were well consistent with those found in the cell morphology assay above. We think that the significant cell apoptosis induction in the BEL-7404 cells by **1** was neither simply by a DNA intercalation action like 9-AIH nor simply by a DNA covalent binding action like cisplatin. It was expected for **1** to exert a synergistic effect for its antitumor activity [35].

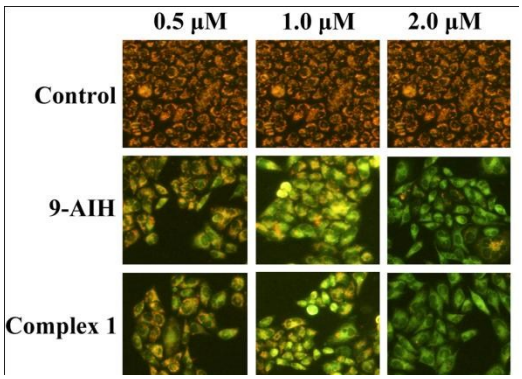

Figure 10. Collapse of mitochondrial membrane potential of BEL-7404 cells treated by 0.5, 1.0 and 2.0 μM of 9-AIH and complex **1** for 24 h, respectively, and stained by JC-1. Selected fields illustrated the corresponding live cells (orange-red), apoptotic cells (green). Images were acquired using a Nikon Te2000 microscope (magnification 200×).

2.8 Inhibition of mutant p53 expression

The p53 gene is regarded to be highly correlated with the occurring of human tumor cells. However, the transformation of p53 gene from the wild type to the mutant type is the most common event in the cancer cells, accounting for at least 50% of all cases [36,37]. The over expression of the mutant p53 will cause the vigorous proliferation of tumor cells, for which the mutant p53 suppression was considered to be an effective antitumor mechanism [38].

From the above results, both **1** and 9-AIH showed significant antiproliferative effects on the BEL-7404 cells, and they also blocked the cell cycle at S phase and G2/M phase, respectively. So the wild-type p53 expression in the BEL-7404 cells was assumed to be inactive and the mutant p53 expression may be also suppressed by **1** or 9-AIH, for which their inhibition effects on the mutant p53 expression were studied by western blotting assay with *β*-actin as the internal reference. As shown in Figure 11, the expression of the mutant p53 protein was heavily suppressed in the presence of **1** or 9-AIH in tumor cells. Comparing with the control, the presence of **1** at 1.0 μM reduced the p53 expression from 100% to 33%, while the 9-AIH also reduced the p53 expression down to 35% under the same condition. These results demonstrated that the inhibition effects of **1** and 9-AIH on the mutant p53 expression highly contributed to their cell growth inhibitions on the BEL-7404 cells, which showed a possible pathway for their antitumor mechanisms.

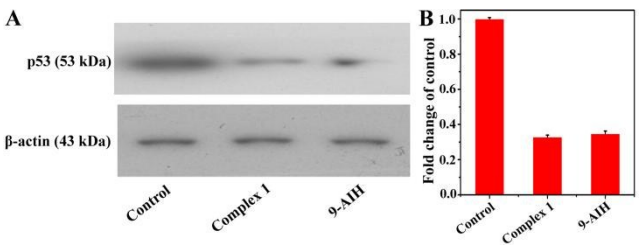

Figure 11. (A) The inhibition effects on the mutant p53 expression in BEL-7404 cells incubated with **1** or 9-AIH at 1.0 μM for 24 h examined by western blotting assay (the 43-kDa *β*-actin used as the internal reference). (B) The histogram representation of the mutant p53 expression inhibited by **1** and 9-AIH, respectively. The relative expression of each band = (OD of each band) / (OD of actin band), while the mean SD was achieved from three independent measurements.

2.10 Assessment on the caspase-9 and caspase-3 activation for cell apoptosis

The caspase is a family of cysteine proteinases existing in the cytoplasm, which are closely correlated with the cell apoptosis *via* the mitochondrial pathway [39]. The caspase-9 and the caspase-3 are the most representative members in the caspase family, the activation of whom will initiate and execute the cell apoptosis, respectively [40]. It should be noted that some anticancer agents that interact with DNA, especially with the mitochondrial DNA, may selectively enhance the generation of ROS in mitochondria and release the cytochrome C based on the loss of mitochondrial membrane potential, which will cause the cell apoptosis by the caspase cascade, including the consequent activation of caspase-9 and caspase-3 [41].

To confirm the detailed antitumor mechanisms involved respectively for **1** and 9-AIH, the representative caspase activity in the BEL-7404 cells was detected by using the colorimetric assay when they were treated with 1.0 μM of **1** and 9-AIH for 12 h and 24 h, respectively. As shown in Figure 12, additional peaks for the activated caspase-9 (FITC-LEHD-FMK probes) and the activated caspase-3 (FITC-DEVD-FMK probes) were obviously detected in the cells treated with **1** for 24 h. Comparing with the control group, the proportions of the activated caspase-9 and caspase-3 induced by **1** increased from 3.2% to 8.7% and 5.7% to 26.3%, respectively. However, no obvious activation on the caspase-9 and caspase-3 induced by **1** for 12 h was observed, as shown in Figure S6, implying the time-dependent activation of the caspase cascade pathway by **1**. Comparatively, there were also no significant changes on the expression levels of the activated caspase-9 and caspase-3 induced by 9-AIH under the same condition (both for 12 h and 24 h), suggesting the apoptotic pathway in the BEL-7404 cells incubated with 9-AIH might not depend on the caspase cascade pathway. Considering the ROS generation was usually occurred in the presence of copper(II) complexes [42,43], the different pathways for the cell apoptosis induced by **1** and 9-AIH should be accepted, even though they showed the same inhibition abilities on the mutant p53 expression.

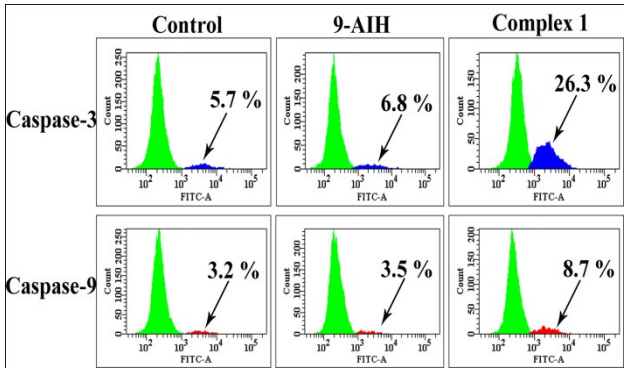

Figure 12. The expression level of caspase-9 and caspase-3 pro-apoptotic protein enhanced in BEL-7404 cells under the treatment of complex **1** and 9-AIH at 1.0 μM for 24 h. Caspase-3 was assessed using the CasPGLOW™ Fluorescein Activite Caspase-3 Staining kit by flow cytometry.

2.11 ROS generation detected by flow cytometry

It is generally regarded that the generation of ROS (reactive oxygen species) by antitumor active compounds may trigger the mitochondrial pathway for cell apoptosis [44,45]. While some other reports demonstrated that the cell apoptosis *via* mitochondrial pathway may be independent of ROS generation [46,47]. The studies above indicated that **1** induced more significant cell apoptosis in BEL-7404 cells comparing with 9-AIH. Whether the more significant antitumor action of **1** can be ascribed to the enhanced ROS generation by **1** is worthy of discussion. As shown in Figure 13, comparing with the control group, the presence of **1** and 9-AIH for 24 h at the IC_{50} concentration of 1.0 μM both enhanced the released ROS level in the BEL-7404 cells. It suggests that the enhanced ROS generation is closely related to the presence of **1** or 9-AIH in cells. Incubation with 9-AIH in BEL-7404 cells led to about 1.7 times of ROS generation higher than the control. However, it clearly showed that **1** could induce the ROS generation more effectively than 9-AIH in BEL-7404 cells, which led to about 3 times of ROS generation comparing with the control under the same condition. It should be ascribed to the copper(II) centre of **1**, which may play a critical role for the antitumor mechanism of **1** *via* the mitochondrial pathway.

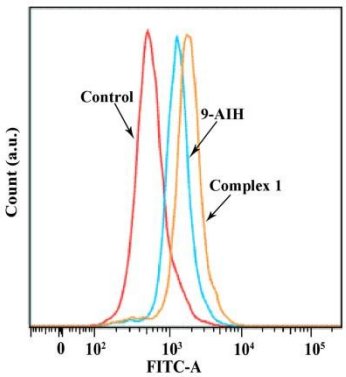

Figure 13. The ROS generation detected by flow cytometry in the BEL-7404 cells incubated with 1.0 μM of 9-AIH and complex **1**, respectively. The ROS level was assessed by examining the fluorescence of DCF in cells by flow cytometry.

2.12 Acute toxicity test for complex 1 *in vivo*

The acute toxicity of complex **1** *in vivo* was assessed on mice by treatment with complex **1** at four doses (45, 40, 32, 22.5 mg/kg) for a 14 days' duration. The numbers of the mice death were recorded and summarized in Table 3. It was found that treatment with **1** at a high dose (45 mg/kg) killed all mice. Comparatively, the mice all survived under the treatment with **1** at 32 mg/kg throughout the 14 days' duration, as the same to the control group. Notably, the mice treated with above dose of **1** showed less action within about 5 hours after injection, and loss their body weight significantly in the next 2 days. The survived mice were sacrificed on day 14 for pathological observation. There were no obvious signs of peritonitis or other damages on the organs of the treated mice, except the slight hepatomegalia in some mice was found. Although the exact LD_{50} value was not easily obtained due to the narrow range for the safety dosage of **1**, it clearly indicated the LD_{50} value of **1** should be in the range of 32~45 mg/kg for this strain of mice.

Table 3. *In vivo* acute toxicity of complex **1** tested on mice.

Duration (days)	Dosage of **1** (mg/kg)				
	45	40	32	22.5	Control
0	8	8	8	8	8
1	1	0	0	0	0
2	5	1	0	0	0
3	1	1	0	0	0
4	1	1	0	0	0
5-14	0	0	0	0	0
Total death	8	3	0	0	0
Death (%)	100	37.5	0	0	0

By contrast, it was found that the tested mice treated with 9-AIH all survived on the gradient dosage of 67.5, 45, 32 mg/kg, respectively. The results suggested that the complex **1** was more like a cytotoxic antitumor agent than 9-AIH by coordinating copper(II) with 9-AIH. However, associated with the moderate cytotoxicity on the normal liver cell line HL-7702 *in vitro* and the slight damage on the liver of mice *in vivo*, it seemed that the liver was not the primary target organ for the high cytotoxicity of **1**, which still needs to be further studied.

3. Experimental section

3.1 Materials and instrumentation

All the chemical reagents were of analytical grade and commercially available. Ethidium Bromide (EB) as DNA intercalative probe was purchased from Biotium. Calf thymus DNA (ct-DNA) was purchased from Sigma-Aldrich. pUC19 plasmid DNA as stock solution of 250 ng/μL was purchased from Takara Biotech. They were all used as received without further purification.

Complex **1** as well as 9-AIH was dissolved in DMSO for the preparation of stock solution at a concentration of 2.0 mM in DNA binding studies. Tris-NaCl buffer solution (5 mM Tris, 50 mM NaCl, adjusted to pH = 7.3 by hydrochloric acid) was prepared using double distilled water. A Tris-buffer solution of ct-DNA gave ratios of UV absorbance at 260 nm to 280 nm as *ca.* 1.85: 1, indicating the DNA was sufficiently free of protein. The DNA concentration per nucleotide was determined spectrophotometrically by employing a molar absorption coefficient of 6600 $M^{-1}cm^{-1}$ at 260 nm.

Infrared spectra were obtained on a PerkinElmer FT-IR Spectrometer. Elemental analyses (C, H, N) were carried out on a PerkinElmer Series II CHNS/O 2400 elemental analyzer. Mass spectra were recorded on a Thermo Fisher Exactive HPLC-MS and a Bruker Daltonics HCT ESI-MS, respectively for 0 h and 24 h incubation. NMR spectra were recorded on a Bruker AV-500 NMR spectrometer. Fluorescence measurements were performed on a Shimadzu RF-5301/PC spectrofluorophotometer.

3.2 Synthesis and characterization of 9-AIH and complex 1

3.2.1 Anthracene-9-imidazoline hydrazone (9-AIH)

9-Anthraldehyde (0.024 mol, 4.944 g) and 2-hydrazino-2-imidazoline hydrobromide (0.024 mol, 4.344 g) were mixed in 80 mL of *n*-butanol in the presence of CH_3COONa (0.024 mol,

1.962 g). The mixture was refluxed under 120 ℃ for 1 h to be dissolved as a yellow solution, along with some white precipitate (NaBr). It was then hot filtered before it was cooled down to room temperature. The yellow precipitate was formed as the product and was then filtered again. The raw product was washed by *n*-butanol and acetone, and was re-crystalized by methanol/chloroform (1:1) to give the anthracene-9-imidazoline hydrazone (9-AIH) in its acetate as pure products ($C_{18}H_{16}N_4$ CH_3COOH, MW = 348 g/mol, yield: 6.105 g, 73%). IR (KBr): 1661, 1519, 1405, 1113 cm^{-1}. ESI–MS m/z: 288.93 $[M–CH_3COO]^+$ (methanol containing 5% DMSO as solvent); Elemental analysis: calcd. (%) for $C_{20}H_{20}N_4O_2$: C 68.95, H 5.79, N 16.08 %; found: C 68.70, H 5.50, N 16.28 %. ^{1}H-NMR (500 MHz, d_6-DMSO) δ 9.17 (s, 1H, ArH), 8.60 (d, 2H, ArH), 8.55 (s, 1H, ArCH=N), 8.06 (d, 2H, ArH),7.53 (m, 4H, ArH), 3.46, (s, 4H, CH_2CH_2), 1.89 (s, 3H, CH_3 of acetate).

3.2.2 The title copper(II) complex (1), *cis*-[$CuCl_2$(9-AIH)]

As shown in Scheme 2, $CuCl_2$ $2H_2O$ (0.2 mmol, 0.048 g) dissolved in 10 mL ethanol was dropwise added into the 30 mL ethanol solution of 9-AIH (0.2 mmol, 0.058 g). The reaction solution was stirred for 24 h in a 60 ℃ water bath, before it was stopped and cooled down to room temperature. Then the filtrated solution was allowed to evaporate slowly for 4–5 days, and the green block crystals suitable for X-ray single-crystal diffraction analysis were harvested (yield: 0.042 g, 45% (noted:)). IR (KBr): 3126, 2906, 2885, 1645, 1619, 1368, 1311, 1289, 1152, 1100, 1064, 1040, 990, 883, 837, 782, 730, 680, 511, 483 cm^{-1}. ESI–MS m/z: 464.05 $[M–Cl+DMSO]^+$ (0 h), 386.4 $[M–Cl]^+$ (24 h) (tris buffer containing DMSO as solvent, as shown in Figure S4). Elemental analysis: calcd. (%) for $C_{18}H_{16}Cl_2CuN_4$ CH_3CH_2OH: C 51.23, H 4.73, N 11.95 %; found: C 51.01, H 4.95, N 11.71 %.

3.3 X-ray crystallography

The data collection of single crystal of complex **1** was performed on an Agilent APEX2 CCD diffractometer equipped with graphite monochromated Mo-Kα radiation (λ = 0.07107 nm) at room temperature. The structure was solved with direct methods and refined using OLEX2 and SHELXL-97 programs [48,49]. The non-hydrogen atoms were located in successive difference Fourier synthesis. The final refinement was performed by full-matrix least-squares methods with anisotropic thermal parameters for no-hydrogen atoms on F^2. The hydrogen atoms were added theoretically and riding on the concerned atoms. The crystallographic data and refinement details of the structure analyses are summarized in Table 1.

3.4 *In vitro* cytotoxicity

The human tumor cell lines (BEL-7404, HepG2, MGC80-3, NCI-H460 and HeLa) and the human normal liver cell line HL-7702 were obtained from Shanghai Cell Bank in Chinese Academy of Sciences. Cisplatin was selected as a reference metallodrug. Each compound was prepared as 2.0 mM DMSO stock solution before they were diluted to 20 μM by PBS buffer (containing 1% DMSO). The cell culture was maintained on RPMI-1640 medium supplemented with 10% fetal bovine serum, 100 U/mL of penicillin and 100 μg/mL of streptomycin in 25 cm^2 culture flasks at 37 °C humidified atmospheres with 5% CO_2. All cells to be tested in the following assays have a passage number of 3~6. 5.0×10^3 cells per well were seeded in triplicate in 96-well plates and incubated for 24 h at 37 ℃ and 5% CO_2/95% air. Then each compound was added to the wells in 10 μL of FBS free culture medium and the plates were incubated in a 5% CO_2 humidified atmosphere for 48 h. Six replica wells were used for controls. Cells were grown for 12 h before treatment to get 70% confluency and 20 μL of the solution of the tested compound was added to each well. The final concentration of the tested compound was kept to 1.25, 2.5, 5, 10, 20 μM, respectively. After 48 h of cultivation, 0.1 mg of MTT (in 20 μL of PBS) was added to each well, and cells were incubated at 37 ℃ for 6 h. The formed formazan crystals were then dissolved in 100 μL of DMSO and the absorbance was read by enzyme labeling instrument with 490 nm/630 nm double wavelength measurement. The final IC_{50} values were calculated by the Bliss method (n = 5). All tests were repeated in at least three independent trials.

3.5. DNA binding studies by spectroscopic analysis

The 2×10^{-3} M ct-DNA stock solution was stored at 4 ℃ for no more than 5 days before use. The synthesized complex **1** and the 9-AIH ligand were all prepared as 2×10^{-3} M DMSO stock solutions for DNA binding studies. The final working solutions were diluted by TBS and the DMSO content was less than 5%. A solution containing 1×10^{-4} M DNA and 1×10^{-5} M EB ([DNA]/[EB] = 10:1) was prepared for the DNA competitive binding studies. Fluorescence emission spectra were recorded under slit width of 5 nm / 5 nm for E_x (350 nm) / E_m (590 nm), respectively. The quenching constant, K_q, for each compound to compare the quenching ability was obtained by the linear fit of plotting I_0/I versus [Q], using the classic Stern–Volmer equation: $I_0/I = 1+K_q\times[Q]$ [50], where I_0 and I referred to the peak emission intensity of the EB-DNA system in the absence and presence of each compound as the quencher, and [Q] is the concentration of the quencher.

3.6. Agarose gel electrophoresis assay

In plasmid DNA unwinding experiments, The DMSO stock solution (2.0 mM) of complex **1** and 9-AIH were both diluted to the concentrations ranged from 25 to 200 μM by TBE buffer (TBE: Tris - Boric acid - EDTA buffer solution). Each compound of gradient concentrations and 0.5 μg DNA were mixed and brought to 25 μL by TBE buffer so that electrophoresis on each sample can be repeated twice. All samples were incubated at 25 °C in the dark for 4 h. Then each sample of 12 μL mixed by 2 μL DNA loading buffer was electrophoresed through 1% agarose gel immersed in TBE buffer for 60 min at 5 V/cm, followed by visualization on a BIO-RAD imaging system under a UV-Vis transilluminator.

3.7 Flow cytometric analysis for cell cycle assay

In the cell cycle analysis, the BEL-7404 cells were maintained with 10% fetal calf serum in 5% CO_2 at 37 °C. Cells were harvested by trypsinization and rinsed with PBS. After centrifugation, the pellet (10^5–10^6 cells) was suspended in 1 mL PBS. The cells were washed in PBS and fixed with ice-cold 70% ethanol in PBS under violent shaking. 1×10^6 cells were centrifuged and re-suspended in a staining solution (0.5 mL of PBS containing 50 μg/mL of PI and 75 kU/mL of RNase A) for 30 min at room temperature in the dark. Finally, the cells were analyzed on a FACS Calibur flow cytometer and a Cell Quest

using ModFit LT for the cell cycle and cell apoptosis studies. The Annexin V-FITC/PI assay was performed as previously described [51]. Briefly, adherent BEL-7404 cells were harvested and suspended in the annexin-binding buffer (5×10^5 cells/mL). Then, cells were incubated with annexin V-FITC and PI for 1.0 h at room temperature in the dark and immediately analyzed by flow cytometry. The data are presented as biparametric dot plots showing PI red fluorescence vs annexin V-FITC green fluorescence.

3.8 Fluorescence morphological examination

Cellular apoptotic morphological changes, which can be detected by Hoechst 33258 staining and AO/EB staining respectively, were studied by fluorescence microscope. To examine whether 9-AIH or complex **1** induce apoptosis in BEL-7404, cells were plated in six-well plates, and treated with 0, 1.0 μM of 9-AIH or complex **1** for 24 h, respectively. For Hoechst 33258 staining, the cells after treatment were washed with PBS and fixed for 10 min at room temperature. The cells were rinsed twice in PBS and stained with Hoechst 33258 fluorescent dye, at room temperature in the dark for 10 min. The cells were then washed twice with PBS, examined and immediately photographed under the fluorescence microscope with excitation wavelength of 330–380 nm. Apoptotic cells were defined based on the nuclear morphology changes such as chromatin condensation and fragmentation. Briefly, the cells were trypsinized and harvested, suspended in PBS, stained by 100 μg/mL of AO/EB for 10 min at room temperature, and were then visualized by the fluorescence microscopy at the excitation wavelength of 545 nm. More than 200 cells in random were assayed.

3.9 Measurement of mitochondrial membrane potential

The loss of mitochondrial membrane potential ($\Delta\psi$) was assessed using a lipophilic cationic fluorescent probe, JC-1 (5,5′,6,6′-tetrachloro-1,1′,3,3′-tetraethylbenzimidazolylcarbocyanine). Cells treated with 0, 0.5, 1.0, 2.0 μM of 9-AIH and complex 1 for 24 h were incubated with 5 μg/mL JC-1 for 20 min at 37 ℃ and examined under the fluorescence microscopy. The emission fluorescence for JC-1 was monitored at 530 and 590 nm, under the excitation wavelength at 488 nm. The orange-red emission of the dye is attributable to a potential-dependent aggregation in the mitochondria, which reflects the $\Delta\psi$. Green fluorescence reflects the monomeric form of JC-1, appearing in the cytosol after mitochondrial membrane depolarization.

3.10 Caspase activity determined by flow cytometric analysis

The BEL-7404 cells of 1×10^6 were cultured for 24 h. After a treatment with 1.0 μM 9-AIH and complex **1** for 12 h and 24 h, respectively, cells were harvested and washed 3 times with cold PBS and were then mixed with 300 μL culture. 1 μL of FITC-DEVD-FMK or FITC-LEHD-FMK was consequently added and incubated for 1.0 h at 37 ℃ with 5% CO_2. The cells were then examined by a FACSAria II flow cytometer equipped with a 488 nm argon laser and results were represented as the percent change on the activity comparing with the untreated control.

3.11 Western blotting assay

The BEL-7404 cells (5×10^5) were cultured on 60 mm dish and incubated overnight before experiments. BEL-7404 cells were respectively treated with 9-AIH (1.0 μM) and complex **1** (1.0 μM) for 24 h. After incubation, cells were harvested and lysed using the lysis buffer (150 mM NaCl, 100 mM Tris-HCl, pH 7.4, 10% glycerol, 1% Triton X-100, 10 mM NaF, 5 mM sodium pyrophosphate, 5 mM sodium orthovanadate, 0.1% SDS) with protease inhibitor. Total protein extracts (50 μg) were loaded onto 12% SDS-polyacrylamide gel, and were then transferred to polyvinylidene fluoride (PVDF) membranes. The membrane was blocked with 5% BSA in TBST buffer and incubated with corresponding primary antibodies at 4 ℃ overnight. Anti-p53, and anti-β-actin were obtained from Abcam. After washing, the membrane was incubated with secondary antibody conjugated with horseradish peroxidase for 120 min. The immune-reactive signals were detected using enhanced chemoluminance kit (Pierce ECL Western Blotting Substrate) following the procedures given in the user's manual.

3.12 Reactive oxygen species (ROS) detection

DCFH-DA is a freely permeable tracer specific for ROS detection. The DCFH-DA in the cells can be de-acetylated by intracellular esterase to the non-fluorescent DCFH, which will be oxidized by ROS to the fluorescent compound, 2',7'-dichloroflorescein (DCF). Therefore, the fluorescence intensity of DCF is proportional to the amount of ROS produced in the cells [52]. In this experiment, 1×10^6 cells were incubated with 1.0 μM (IC_{50} concentration) of 9-AIH and complex **1** for 24 h, respectively. After the exposure, cells were harvested, washed with ice-cold PBS once and incubated with 100 μM of DCFH-DA (100 μM in a final concentration) at 37 ℃ for 15 min in the dark. Finally, the cells were washed again and maintained in 1 mL PBS. The ROS generation was assessed using flow cytometry by examining the fluorescence of DCF in cells for each sample collected from 1×10^6 cells.

3.13 *In vivo* acute toxicity evaluation

All the tests were carried out in the animal experimental centre of Guangxi Medical University. Male and female KM mice (5-6 weeks old, 20-23 g weight) were housed in a specific pathogen free facility with conditions of constant photoperiod (12 h light / 12 h dark with 25~28 ℃ temperature and 45~65% humidity). Groups of mice (n = 8 per group) were injected intraperitoneally with a single dose of 45, 40, 32, and 22.5 mg/kg, respectively, comparing with the control group, according to our pilot study. The mice were daily observed for the signs of toxicity and mortality throughout the 14 days' duration. The tested compound for injection was dissolved in a mixture of DMSO and 0.9% saline (10% / 90%, V/V) for ip administration, while the control group received the same volume of solvent.

Conclusions

In this work, an anthracycline derivative, anthracene-9-imidazoline hydrazone (9-AIH), was synthesized and selected as an antitumor active ligand to afford the first copper(II) complex **1** of 9-AIH. 9-AIH alone exhibited moderate *in vitro* antitumor activity, while **1** showed better activities than 9-AIH by combining this ligand with copper(II). From the results of the flow cytometry, complex **1** and 9-AIH blocked the cell cycle and induced the cell apoptosis in the BEL-7404 cells in different

stages. It suggested their different antitumor mechanisms, even though they both induced the cell apoptosis in dose-dependent manner *via* the ROS-related mitochondrial pathway. However, **1** exhibited higher efficiency in this antitumor mechanism, which finally appeared as the higher release of ROS. And as a result, **1** could suppress the mutant p53 protein expression and activate the caspase-9 / 3 for the caspase cascade more effectively than 9-AIH. However, the *in vivo* acute toxicity test indicated that the formation of this copper(II) complex of 9-AIH not only enhanced its antitumor efficacy, but also its cytotoxicity both *in vitro* and *in vivo*. So from this study, it can be confirmed that complex **1** has been developed into a cytotoxic antitumor agent by coordinating copper(II) with 9-AIH, in which the Cu(II) centre should play a crucial role for the boon and bane on the cytotoxicity of **1**. However, the bioactivity of Cu(II) was emphasized again through this study, which still directed a promising way to achieve new antitumor metallodrugs with better efficacies.

Acknowledgement

This work was supported by Natural Science Foundation of China (Nos. 21271051, 81473102, 21431001), IRT1225, Natural Science Foundation of Guangxi Province (No. 2013GXNSFAA019044), Foundation of State Key Laboratory Cultivation Base for the Chemistry and Molecular Engineering of Medicinal Resources (CMEMR2012-A11/2013-C05) as well as "BAGUI Scholar" program of Guangxi Province of China.

Notes and references

[a] *State Key Laboratory Cultivation Base for the Chemistry and Molecular Engineering of Medicinal Resources; School of Chemistry and Pharmaceutical Sciences, Guangxi Normal University, Guilin 541004, P. R. China.;*
Fax: 086-773-2120958; Tel: 086-773-2120998;
E-mail: ycliugxnu@aliyun.com (Y.–C. Liu); hliang@gxnu.edu.cn (H. Liang)

§ Electronic Supplementary Information (ESI) available:
Crystallographic data for the structural analysis have been deposited in the Cambridge Crystallographic Data Centre, CCDC No. 1036794 for complex **1**. The data can be obtained free of charge via http://www.ccdc.cam.ac.uk, or from the Cambridge Crystallographic Data Centre, 12 Union Road, Cambridge CB21EZ, UK; fax: (+44) 1223-336-033; or e-mail:deposit@ccdc.cam.ac.uk.
See DOI:

‡ Footnotes should appear here. These might include comments relevant to but not central to the matter under discussion, limited experimental and spectral data, and crystallographic data.

References

1 F. –M. Arcamone, Anthracyclines, *Anticancer agents from natural products (2nd Edition by D. J. Cragg, G. M. Kingston, D. G. I. Newman), CRC Press*, 2011, Chap. **16**, 383-406.
2 G. Minotti, P. Menna, E. Salvatorelli, G. Cairo and L. Gianni, Anthracyclines: Molecular advances and pharmacologic developments in antitumor activity and cardiotoxicity, *Pharmacol. Rev.*, 2004, **56**(2), 185-229.
3 R. Kizek, V. Adam, J. Hrabeta, T. Eckschlager, S. Smutny, J. V. Burda, E. Frei and M. Stiborova, Anthracyclines and ellipticines as DNA-damaging anticancer drugs: Recent advances, *Pharmacol. Therapeut.*, 2012, **133**(1), 26-39.
4 S. Toldo, R W Goehe, M Lotrionte, E. Mezzaroma, E. T. Sumner, G. G. L. Biondi-Zoccai, I. M. Seropian, B. W. Van Tassell, F. Loperfido, G. Palazzoni, N. F. Voelkel, A. Abbate and D. A. Gewirtz, Comparative cardiac toxicity of anthracyclines *in vitro* and *in vivo* in the mouse, *PLoS ONE*, 2013, **8**(3), e58421
5 G. Visani, A. Isidori and G. Minotti, Cardiomyopathies- From basic research to clinical management: Chapter 27, Anthracycline cardiotoxicity (edited by J. Veselka), *InTech*, **2012**, 621-644.
6 A. Romero, T. Caldés, E. Díaz-Rubio and M. Martín, Topoisomerase 2 alpha: a real predictor of anthracycline efficacy? *Clin. Transl. Oncol.*, 2012, **14**(3), 163-168.
7 C. Duncan and A. R. White, Copper complexes as therapeutic agents, *Metallomics*, 2012, **4**, 127-138.
8 H. Sun, Z. Yu, W. –Q. Yang, W. –J. He and Z. –J. Guo, Oxidative DNA cleavage mediated by copper complexes, *Chem. J. Chin. Univ.*, 2011, **32**(3), 437-450.
9 D. B. Lovejoy, P. J. Jansson, U. T. Brunk, J. Wong, P. Ponka and D. R. Richardson, Antitumor activity of metal-chelating compound Dp44Mt is mediated by formation of a redox-active copper complex that accumulates in lysosomes. *Cancer Res.*, 2011, **71**(17), 5771-5880.
10 S. Boutaleb-Charki, C. Marín, C. R. Maldonado, M. J. Rosales, J. Urbano, R. Guitierrez-Sánchez, M. Quirós, J. M. Salas and M. Sánchez-Moreno. Copper(II) complexes of [1,2,4] triazolo [1,5-a] pyrimidine derivatives as potential anti-parasitic agents. *Drug. Metab. Lett.*, 2009, **3**(1), 35-44.
11 I. Kostova and L. Saso, Advances in research of Schiff-base metal complexes as potent antioxidants, *Curr. Med. Chem.*, 2013, **20**(36), 4609-4632.
12 K. Sztanke, A. Maziarka, A. Osinka and M. Sztanke, An insight into synthetic Schiff bases revealing antiproliferative activities in vitro, *Bioorg. Med. Chem.*, 2013, **21**, 3648-3666.
13 R. F. Brissos, E. Torrents, F. M. dos Santos Mello, W. C. Pires, E. de Paula Silveira-Lacerda, A. B. Caballero, M. Caubet, C. Massera, O. Roubeau, S. J. Teat and P. Gamez, Highly cytotoxic DNA-interacting copper(II) coordination compounds, *Metallomics*, 2014, **6**, 1853-1868.
14 P. U. Maheswari, S. Barends, S. Ozalp-Yaman, P. de Hoog, H. Casellas, S. J. Teat, C. Massera, M. Lutz, A. L. Spek, G. P. van Wezel, B. Kozlevcar, P. Gamez and J. Reedijk, The square-planar cytotoxic [Cu^{II}(pyrimol)Cl] complex acts as an efficient DNA cleaver without reductant, *J. Am. Chem. Soc.*, 2006, **128**(3), 710-711.
15 X. Qiao, Z. Y. Ma, C. Z. Xie, F. Xue, Y. W. Zhang, J. Y. Xu, Z. Y. Qiang, J. S. Lou, G.-J. Chen and S. P. Yan, Study on potential antitumor mechanism of a novel Schiff Base copper (II) complex: synthesis, crystal structure, DNA binding, cytotoxicity and apoptosis induction activity, *J. Inorg. Biochem.*, 2011, **105**(5), 728-737.
16 C. Núñez, J. F. Lodeiro, M. Diniz and M. Galesio, Versatile Schiff-base hydrazone fluorescent receptors: Synthesis, spectroscopy and complexation studies, *Inorg. Chim. Acta*, 2012, **380**, 40-49.
17 C. Rajarajeswari, R. Loganathan, M. Palaniandavar, E. Suresh, A. Riyasdeen and M. A. Akbarsha, Copper(II) complexes with 2NO and 3N donor ligands: synthesis, structure and chemical nuclease and anticancer activities, Dalton Trans., 2013, **42**, 8347-8363.
18 H. Fei, R. Cao, J.-L. Jia, X.-C. Ma and M. Zhou, Membrane localized iridium(III) complex induces endoplasmic reticulum stress and mitochondria-mediated apoptosis in human cancer cells. *J. Med. Chem.* 2013, **56**(9), 3636-3644.
19 H. –K. Liu and P. J. Sadler, Metal complexes as DNA intercalators, *Acc. Chem. Res.*, 2011, **44**(5), 349-359.
20 L. Strekowski and B. Wilson, Noncovalent interactions with DNA: An overview. *Mutat. Res. – Fund. Mol. M.*, 2007, **623**(1), 3-13.
21 B. M. Zeglis, V. C. Pierre and J. K. Barton, Metallo-intercalators and metallo-insertors, *Chem. Commun.*, 2007 (44), 4565-4579.
22 C. Sissi, L. Bolgan, S. Moro, G. Zagotto, C. Bailly, E. Menta, G. Capranico, and M. Palumbo, DNA-binding preferences of bisantrene analogues: Relevance to the sequence specificity of drug-mediated topoisomerase II poisoning, *Mol. Pharm.*, 1998, **54**(6), 1036-1045.
23 M. Kožurková, D. Sabolová, H. Paulíková, L. Janovec, P. Kristian, M. Bajdichová, J. Buša, D. Podhradský and Ján Imrich, DNA binding properties and evaluation of cytotoxic activity of 9,10-bis-N-substituted (aminomethyl)anthracenes, *Int. J. Biol. Macromol.*, 2007, **41**(4), 415-422.

24 D.-L. Ma and C.-M. Che, A Bifunctional Platinum (II) Complex Capable of Intercalation and Hydrogen-Bonding Interactions with DNA: Binding Studies and Cytotoxicity, *Chem Eur J.*, 2003, **9**(24), 6133-6144.

25 http://biotium.com/product/gelredtm-nucleic-acid-gel-stain-10000x-in-water/

26 G. Zhang, J. Guo, N. Zhao and J. Wang, Study of interaction between kaempferol–Eu^{3+} complex and DNA with the use of the Neutral Red dye as a fluorescence probe, *Sensors and Actuators B: Chem.*, 2010, **144**(1), 239-246.

27 J. R. Lakowicz, Principles of Fluorescence Spectroscopy (3rd Ed.), *Springer-Verlag*, **2006**, pp278-280.

28 J. –W. Liang, Y. Wang, K. –J. Du, G. –Y. Li, R. –L. Guan, L. –N. Ji and H. Chao, Synthesis, DNA interaction and anticancer activity of copper(II) complexes with 4′-phenyl-2,2′:6′,2″-terpyridine derivatives, *J. Inorg. Biochem.*, 2014, **141**, 17-27.

29 V. M. Manikandamathavan, B. U. Nair, DNA binding and cytotoxicity of copper(II) imidazole terpyridine complexes: Role of oxyanion, hydrogen bonding and π-π interaction, *Eur. J. Med. Chem.*, 2013, **68**, 244-252.

30 Z. –F. Chen, Y. –C. Liu, Y. Peng, X. Hong, H. –H. Wang, M. –M. Zhang and H. Liang, Synthesis, characterization, and in vitro antitumor properties of gold (III) compounds with the traditional Chinese medicine (TCM) active ingredient liriodenine, *J. Biol. Inorg. Chem.*, 2012, **17**(2), 247-261.

31 S. Bhattacharyya, A. Sarkar, S. K. Dey, G. P. Jose, A. Mukherjee and T. K. Senqupta, Copper(II) complex of methionine conjugated bis-pyrazole based ligand promotes dual pathway for DNA cleavage, *Dalton Trans.*, 2013, **42**, 11709-11719.

32 P. G. Baraldi, A. Bovero, F. Fruttarolo, D. Preti, M. A. Tabrizi, M. G. Pavani and R. Romagnoli, DNA minor groove binders as potential antitumor and antimicrobial agents, *Med. Res. Rev.*, 2004, **24**(4), 475-528.

33 B. Zhivotovsky and S. Orrenius, Cell cycle and cell death in disease: past, present and future, *J. Intern. Med.*, 2010, **268**, 395-409..

34 D. R. Green and J. C. Reed, Mitochondria and apoptosis, *Science*, 1998, **281**(5381), 1309-1311.

35 W. Zhou, X. Wang, M. Hu, C. Zhu and Z. Guo, A mitochondrion-targeting copper complex exhibits potent cytotoxicity against cisplatin-resistant tumor cells through multiple mechanisms of action, *Chem. Sci*,, 2014, **5**, 2761-2770.

36 P. A. J. Muller, K. H. Vousden and J. C. Norman, p53 and its mutants in tumor cell migration and invasion, *J. Cell Biol.*, 2011, **192**(2), 209-218.

37 A. H. Stegh, Targeting the p53 signaling pathway in cancer therapy – the promises, challenges and perils, *Expert Opin. Ther. Tar.*, 2012, **16**(1), 67-83.

38 M. Oren and V. Rotter, Mutant p53 gain-of-function in cancer, *Cold Spring Harb. Perspect. Biol.*, 2010, **2**: a001107.

39 K. Hara, E. Kasahara, N. Takahashi, M. Konishi, J. Inoue, M. Jikumaru, S. Kubo, H. Okamura, E. Sato and M. Inoue, Mitochondria determine the efficacy of anticancer agents that interact with DNA but not the cytoskeleton. *J. Pharmacol. Exp. Ther.*, 2011, **337**(3), 838-845.

40 G. S. Salvesen and S. J. Riedl, Caspase mechanisms, *Adv. Exp. Med. Biol*., 2008, **615**, 13–23.

41 D. R. Mcllwain, T. Berger and T. W. Mak, Caspase functions in cell death and disease, *Cold Spring Harb. Perspect. Biol.*, 2013, **5**: a008656.

42 C. H. Ng, S. M. Kong, Y. L. Tiong, M. J. Maah, N. Sukram, M. Ahmad and A. S. B. Khoo, Selective anticancer copper(II)-mixed ligand complexes: targeting of ROS and proteasomes. *Metallomics*, 2014, **6**(4), 892-906.

43 A. G. R. Despaigne, J. G. Da Silva, P. R. da Costa, R. G. dos Santos and H. Beraldo, ROS-mediated cytotoxic effect of copper(II) hydrazone complexes against human glioma cells. *Molecules*, 2014, **19**(11), 17202-17220.

44 K. Sinha, J. Das, P. B. Pal and P. C. Sil, Oxidative stress: the mitochondria-dependent and mitochondria-independent pathways of apoptosis, *Arch. Toxicol.*, 2013, **87**(7), 1157-1180.

45 P. Li, Q. –L. Zhao, L. –H. Wu, P. Jawaid, Y. –F. Jiao, M. Kadowaki and T. Kondo, Isofraxidin, a potent reactive oxygen species (ROS) scavenger, protects human leukemia cells from radiation-induced apoptosis via ROS/mitochondria pathway in p53-independent manner. *Apoptosis*, 2014, **19**, 1043-1053.

46 T. Arimura, A. Kojima-Yuasa, D. O. Kennedy and I. Matsui-Yuasa, Reactive oxygen species-independent G1 arrest induced by evening primrose extract in Ehrlich ascites tumor cells. *Cancer Lett.*, 2004, **207**(1), 19-25.

47 C. H. Ko, S. C. Shen, C. S. Hsu and Y. C. Chen, Mitochondrial-dependent, reactive oxygen species-independent apoptosis by myricetin: roles of protein kinase C, cytochrome C, and caspase cascade. *Biochem. Pharmacol.*, 2005, **69**(6), 913-927.

48 O. V. Dolomanov, L. J. Bourhis, R. J. Gildea, J. A. K. Howard and H. Puschmann, OLEX2: a complete structure solution, refinement and analysis program. *J. Appl. Cryst.*, 2009, **42**(2), 339-341.

49 G. M. Sheldrick, SHELXS97 and SHELXL97, *University of Gӧttingen*, Germany, **1997**.

50 C. V. Kumar and E. H. Asuncion, DNA binding studies and site selective fluorescence sensitization of an anthryl probe. *J. Am. Chem. Soc.*, 1993, **115**(19), 8547-8553.

51 Z. –F. Chen, Q. –P. Qin, J. –L. Qin, Y. –C. Liu, K. –B. Huang, Y. –L. Li, T. Meng, G. –H. Zhang, Y. Peng, X. –J. Luo and H. Liang, Stabilization of G-quadruplex DNA, inhibition of telomerase activity, and tumor cell apoptosis by organoplatinum(II) complexes with oxoisoaporphine, *J. Med. Chem.*, 2015, **58**, 2159-2179.

52 L. Bourré, S. Thibaut, A. Briffaud, N. Rousset, S. Eléouet, Y. Lajat and T. Patrice, Indirect detection of photosensitizer ex vivo, *J. Photoch. Photobio B*, 2002, **67**, 23-31.